WILEY VCH

RESEARCH ARTICLE

Electrochemical Exfoliation of Graphene Oxide: Unveiling Structural Properties and Electrochemical Performance

Eduart Gutiérrez-Pineda,*[a,b] Ahmed Subrati,[a] María José Rodríguez-Presa,[c] Claudio A. Gervasi,[c,d] and Sergio E. Moya*[a]

[a] Dr. E. Gutiérrez-Pineda, Dr. A. Subrati, Dr. S.E. Moya
Soft Matter Nanotechnology Group
CIC biomaGUNE
Paseo Miramon 182 C, 2009 San Sebastián, Gipuzkoa, Spain
E-mail: smoya@cicbiomagune.es, egutierrez@cicbiomagune.es

[b] Dr. E. Gutiérrez-Pineda
Escuela de Ciencias Básicas, Tecnología e Ingeniería (ECBTI)
Universidad Nacional Abierta y a Distancia (UNAD)
Bucaramanga, Santander 680001, Colombia

[c] Dr. M. J. Rodríguez-Presa, Dr. C. A. Gervasi
Instituto de Investigaciones Fisicoquímicas Teóricas y Aplicadas (INIFTA)
Universidad Nacional de La Plata – CONICET
Sucursal 4 Casilla de Correo 16, 1900 La Plata, Argentina

[d] Dr. C. A. Gervasi
Área Electroquímica, Depto. Ing. Qca., Facultad de Ingeniería
Universidad Nacional de La Plata
La Plata (1900), Argentina

Supporting information for this article is given via a link at the end of the document.

Abstract: An electrochemical exfoliation method for the production of graphene oxide and its characterization by electrochemical techniques are presented here. Graphite rods are used as working electrode in a three-electrode electrochemical cell, and electro-exfoliation is achieved by applying anodic polarization in a sulfuric acid solution. The electrochemical process involved two steps characterized by an intercalation at lower potential and an exfoliation at higher potential. The electrochemical behavior of the produced GO is studied through cyclic voltammetry (CV) and electrochemical impedance spectroscopy (EIS). X ray Photoelectronic Spectroscopy (XPS), Raman spectroscopy, Transmission Electron Microscopy (TEM), and Atomic Force Microscopy (AFM) are employed to characterize the structural and chemical properties of the exfolieted GO. The results demonstrate that the electrochemical exfoliation method yields GO materials with varying degrees of oxidation, defect density, and crystallite size, depending on the applied potential and acid concentration. The graphene oxide samples exhibited distinct electrochemical properties, including charge transfer resistance, interfacial capacitance, and relaxation times for the charge transfer, as revealed by CV and EIS measurements with a specifically selected redox probe. The comprehensive characterization performed provides valuable insights into the structure-property relationships of the GO materials synthesized through electrochemical exfoliation of graphite.

Introduction

Carbonaceous compounds are a fascinating class of materials, which are primarily formed by carbon atoms. They exhibit a wide range of physical and chemical properties that have generated large interest from a technological and scientific perspective due to the numerous applications that can be derived from these materials.[1–3] Graphene and Graphene Oxide (GO) have emerged as prominent examples of these materials due to their unique characteristics and versatility in scientific and technological applications.[4,5] Graphene is a two-dimensional (2D) material with a single layer of carbon atoms arranged in a hexagonal structure through sp^2 bonds.[6] Since its discovery in 2004 this material has captured the scientific community's attention due to its extraordinary properties. It possesses high electrical conductivity (0.60×10^8 Ω^*cm^{-1}) and thermal conductivity (4000 $Wm^{-1}K^{-1}$),[7] exceptional mechanical strength (130 GPa),[8] and large specific surface area (2,629 m^2/g).[9] Its various fields of application include electronic devices, energy storage, catalysis, and composite materials.[4,5,10–13] Regarding its high electrical conductivity, electrons in graphene behave as massless particles that move through the crystalline structure at relativistic speeds.[14] This property has led to the development of high-speed and low-resistance electronic devices based on graphene.

GO is a derivative of graphene in which the surface of the graphene sheet is modified by incorporating oxygenated functional groups, such as hydroxyls, carboxyls, and epoxides.[15,16] This chemical modification gives additional properties and increased solubility in water and other polar solvents.[17] GO retains many attractive properties of graphene, such as its high mechanical strength and large surface area. However, it exhibits lower electrical conductivity due to the introduction of defects and changes in the C hybridization to sp^3 through the introduction of the oxygenated functional groups, which decrease electron mobility.[18,19] Despite this, GO retains interesting conductivity values and can be used in many applications as graphene. GO is of great interest for manufacturing materials related to energy storage,[20] sensors,[4] and biosensors.[10] Similarly, it is also a promising candidate for preparing graphene-like paper materials.[21,22] More importantly, GO is considered a promising precursor for the large-scale

production of graphene-based materials due to its relatively low synthesis cost.

Currently, GO produced on a lab-scale and, in some cases, on an industrial scale is obtained through chemical oxidation of graphite (flakes, powders, bars) using concentrated acids e.g., H_2SO_4, H_3PO_4, HNO_3 and strong oxidizing agents such as $KMnO_4$ or $KClO_3$, following various methodologies such as those by Brodie, Staudenmaier, or Hummers.[23–25] Although widely studied and optimized, these methods generate a considerable environmental impact after scaling up. The use of strong oxidants, such as $KMnO_4$, not only complicates the removal of metal ions from GO but also causes permanent defects that cannot be restored by GO reduction. Electrochemical oxidation has recently been explored as a fresh approach to produce GO due to its moderate environmental impact and low cost.[26–28] Electrochemical exfoliation offers a novel and effective methodology for the manufacture of graphene and GO in large quantities and with precise control over its quality and morphology. Unlike traditional mechanical or chemical exfoliation methods, electrochemical exfoliation makes use of electrochemical reactions to separate (intercalation) and release (exfoliation) graphene oxide layers from a carbon precursor. Electrochemical exfoliation is one of the few potentially cost-effective and scalable methods to convert graphite into GO and graphene.[29–33] As an essentially wet chemical approach, electrochemical methods have the advantage of being environmentally friendly (avoiding hazardous or energy-intensive processes), using low-cost and readily available precursors, and allowing a high degree of functionalization.

This exfoliation process is carried out in an electrochemical cell, where the carbon precursor is used as the working electrode immersed in a suitable electrolyte. Electrolysis occurs under anodic or cathodic polarization, which drives electrochemical reactions that, in turn, promote the exfoliation of the material and the transfer of graphene layers to the electrolyte.[13,28] The choice of a specific electrolyte can control the rate and efficiency of exfoliation and influence the quality and characteristics of the graphene-type materials obtained.[34,35] Anodic conditions, with potentials ranging between 1 - 20 V have been employed in the presence of negative intercalation ions such as SO_4^{2-}, NO_3^-, Cl^- among others.[35–37] This process produces large quantities of GO with a high degree of defects compared to the use of cathodic conditions (negative overpotentials) and positively charged intercalation ions that produce higher-quality graphene, avoiding the formation of oxygen groups on the surfaces but with lower yields.[38,39] Electrochemical exfoliation producing graphene offers several significant advantages compared to other production methods. In addition to enabling large-scale production, this approach is also more environmentally friendly and requires fewer toxic chemicals. Furthermore, precise control of the electrochemical conditions allows adjusting the properties of the resulting graphene to suit various applications, such as electronic devices, energy storage, sensors, and composite materials. Despite all the advantages mentioned above and the efforts to optimize the parameters of the process, electrochemical exfoliation still needs to be optimized for large-scale GO production with high yield and control over the degree of oxidation.

This work aims to contribute to a fast and high-yield GO production through a one-pot synthesis by using a two-step anodic process (intercalation and exfoliation) under moderate reaction conditions. In this study, the electrochemical synthesis of GO was performed by using a graphite rod subjected to successive stages of electrochemical intercalation and exfoliation in diluted H_2SO_4 solutions of different concentrations. Different intercalation potential (E_I) and exfoliation potential (E_E) conditions were tested, as well as different time frames for each stage. The morphological and structural characteristics of the obtained electro-exfoliated GO (EGO) were studied by using Transmission Electron Microscopy (TEM), X-ray Photoelectron Spectroscopy (XPS), and Raman Spectroscopy. Subsequently, glassy carbon electrodes (GCE) were modified with EGO suspensions in water as per the film-forming “drop casting” technique. The electrochemical activity of the modified electrodes was evaluated by using the ferrocyanide-ferricyanide redox probe and cyclic Voltammetry (CV) and Electrochemical Impedance Spectroscopy (EIS) techniques. A novel and simple qualitative analysis is proposed, which allows for rapid and accurate ranking of samples based on their electrocatalytic capacity as evidenced by the relaxation times for the charge transfer. These results are compared with the voltammetric analysis in terms of peak potential difference (ΔE_p), while improvements of the proposed method regarding precision and feasibility are discussed.

Results and Discussion

A conventional three-electrode electrochemical cell was employed to produce graphene oxide (GO) via electro-exfoliation of graphite rods. These rods served as the working electrodes. The electro-exfoliation process involved a two-step routine employing a combination of anodic potentials and different H_2SO_4 concentrations (Table 1). Initially, a potential step was applied to the working electrode for 5 minutes to facilitate charge accumulation around the graphite electrode and the intercalation of ions on its surface.[39] This step amplitude will be referred to as the intercalation potential (E_I). Subsequently, the electrode potential was increased for 5 minutes, allowing the anions in the solution to access the intercalation sites and trigger the exfoliation of GO flakes.[28] From this point onward, the step amplitude of the second stage will be referred to as the exfoliation potential (E_E). The negative sulfate ions (SO_4^{2-}) or the traces of hydroxide ions (OH^-) are attracted to the positive anode. However, the sulfate ion is too stable to be oxidized in an aqueous solution. Instead, hydroxide ions or water molecules become oxidized to form oxygen.

When an anodic potential is applied to graphite in H_2SO_4 solution, several stages occur associated with the intercalation-exfoliation process. In the first stage, charge accumulation is generated around the graphite electrode followed by the oxidation of water from the aqueous solution. These accumulated charges create an electric field on the surface of the graphite, enabling the adsorption of sulfate ions at the intercalation sites of graphite. As the anodic potential increases, the sulfate ions present in the solution move toward the intercalation sites in the graphite, where they are inserted between the layers of carbon atoms (graphite intercalation compound with sulfuric acid H_2SO_4-GIC).[29] This insertion of sulfate ions between the graphite layers leads to an expansion of the graphite structure that enables exfoliation of GO into the solution.

Table1. Experimental conditions for the intercalation-exfoliation process

Treatment	E_I (V *vs.* Ag/AgCl)	E_E (V *vs.* Ag/AgCl)	H_2SO_4 (mol*L^{-1})
T1	1,5	3	0,05
			0,1
			0,5
T2	1,5	3,5	0,05
			0,1
			0,5
T3	2	3	0,05
			0,1
			0,5
T4	2	3,5	0,05
			0,1
			0,5

The Intercalation-Exfoliation (I-E) process was repeated for five cycles (for a total time of 50 minutes), as illustrated by chronoamperometric results shown in Figure 1. This study explored various E_I and E_E in combination with different H_2SO_4 concentrations, according to treatments T1 through T4 as shown in Figure 1 and outlined in Table 1. The electrochemical intercalation of SO_4^{2-} into graphite, followed by the exfoliation of GO, was accomplished as described earlier by applying a potentiostatic technique in H_2SO_4 solutions of 0.05 M, 0.1 M, and 0.5 M. Figure 1 illustrates the current-time transients observed during the anodic potential double-step experimental routine, where noticeable current oscillations can be observed. These oscillations in the current transients can be attributed to the repetitive exfoliation of graphene sheets from the graphite surface and the formation of a fresh surface interacting with the electrolyte during the intercalation of SO_4^{2-} into the graphite electrode. [34,36]

These current oscillations (showing in detail in Figure S1) indicate the multistep character of H_2SO_4-GIC transformation into the EGO. Successive transient current spikes are also detected during the occurrence of an electrochemical reaction producing nucleation of gas bubbles on the electrode surface and their subsequent removal after growth.[40] The whole process is related to a rapid decrease in the electroactive area during the growth of bubbles attached to the electrode followed by an instant increase in electroactive area when the bubbles become detached. Current oscillations with high frequency (repeated spikes in succession as a function of time) are observed for each applied potential step during electro-exfoliation of graphite (Figure S1). These oscillations can be understood in a similar way as that described above for a gas evolving event. During the formation of graphene sheets the electroactive area increases (since the final area is the sum of the exposed area of each growing sheet and the newly exposed area on the electrode surface). This condition proceeds until the electrical contact between flake and electrode becomes interrupted. Flake detachment from the surface interrupts the electrical contact resulting in a sudden decrease in the electroactive surface and so, in the measured current. Beck et al. explained the occurrence of potentiostatic oscillations during the galvanostatic oxidation of graphite in terms of a zone model.[41] Recently, Gurzeda et al. similarly observed these oscillations through electrochemical overoxidation of natural graphite in H_2SO_4 using the linear sweep voltammetry (LSV) technique. They proposed a probable mechanism for the oscillatory reactions.

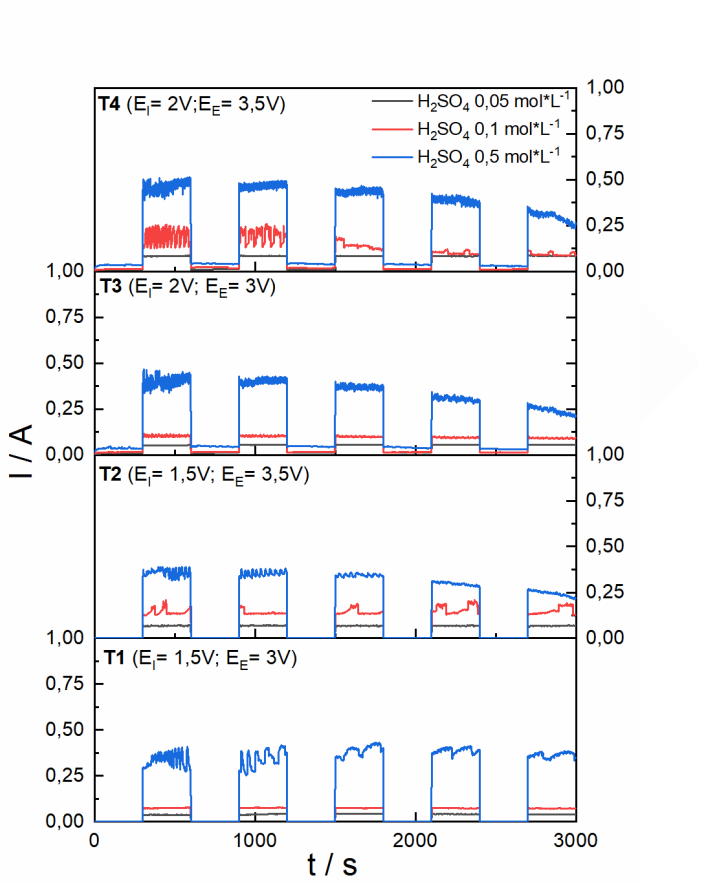

Figure 1. Current–time (I-t) transients recorded for Intercalation-Exfoliation cycles of GO from SO_4^{2-} -intercalated graphite according to four sets of experimental conditions of treatments T1 through T4.

When the critical potential is reached, the co-intercalation of water molecules takes place, followed by their transformation into vicinal OH groups. This electrochemical behaviour is demonstrated by the rise in recorded current. Upon further oxidation, the vicinal OH groups undergo the formation of carbonyl and/or epoxy groups. Consequently, the current starts to decline.[42]

Thus, the size of the current spikes recorded in each cycle results from changes in the active surface area. Furthermore, we observed that below 2V *vs*. Ag/AgCl (KCl 3M) the intercalation step results in yields with low efficiency for the global process and that the current value increases with higher potentials (E_E), indicating an enhancement in SO_4^{2-} intercalation at elevated potentials with the resulting increase in the graphite surface area due to the exfoliation of GO flakes, as reported in previous literature.[43–45] The method proposed in this study offers several advantages over traditional and other electrochemical methods. It operates under moderate reaction conditions, requires short processing times, is relatively cost-effective, and is environmentally friendly, as it avoids generating toxic or hazardous waste. The obtained EGO flakes were subsequently washed, collected, and redispersed in water through sonication. The yield of the exfoliated EG flakes was between 40 - 90% relative to the total weight of the starting graphite electrode and the treatment applied. After applying the electro-exfoliation

technique, we proceeded with a comprehensive characterization of the electrochemically exfoliated graphene oxide (EGO) sheets to evaluate possible structural and chemical differences relatable to the employed I-E conditions.

We carried out TEM and AFM studies to obtain morphological information about graphene sheets. TEM images obtained for EGO materials provide crucial insight into the structural characteristics at the atomic scale. Figures 2 and S2 show representative TEM images recorded after electrochemical treatment at different E_I and E_E. The EGO flakes are discernible in the TEM images as thin, transparent sheets with a layered structure. Dark contrasting areas within the flakes may correspond to the presence of carbon atoms in thicker stacks of multiple EGO layers, while the lighter regions represent voids or inserted species resulting from the intercalation of sulfate ions.[46] The layers of EGO appear to be stacked randomly and irregularly which points out to the effectiveness of the applied exfoliation process in separating EGO layers. Additionally, the TEM images reveal the presence of defects such as wrinkles, folds, and irregular edges within the EGO flakes (Figure S2a-l). These defects result from the exfoliation process and the restructuring of the GO layers during intercalation.[47]

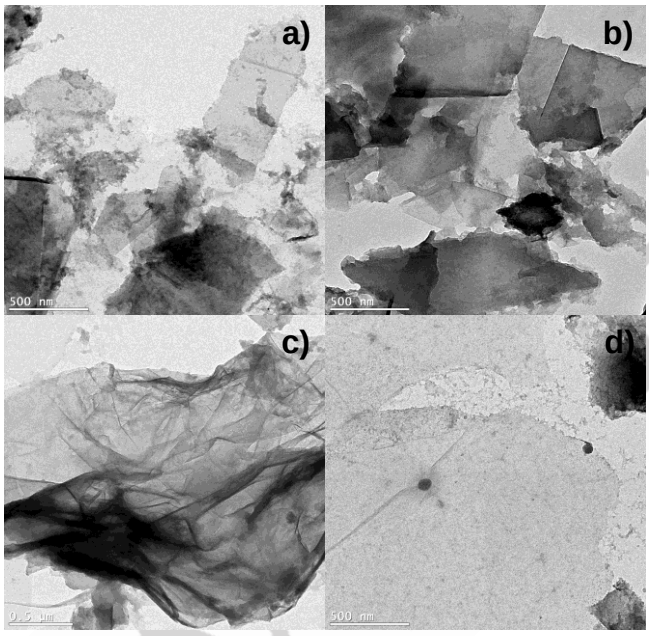

Figure 2. TEM images showing the variety of EGO generated by electrochemical Intercalation-Exfoliation of graphite **a)** T1 (E_I 1.5V; E_E 3V in H_2SO_4 0.05 M) **b)** T2 (E_I 1,5V; E_E 3,5V in H_2SO_4 0,1M) **c)** T13 (E_I 2V; E_E 3V in $H_2SO_4$0,5M) and **d)** T4 (E_I 2V; EE 3,5V in H_2SO_4 0,5M)

TEM images of EGO flakes on a copper grid, prepared at distinct conditions of E_I and E_E, are shown in Figures 2 and S2. As observed in these figures, the variation in I-E potentials results in different transmission and shapes. In all the images, EGO flakes are stacked together, revealing a multi-layered structure. Disordered and relatively thick graphene flakes are observed for EGO flakes prepared at E_I 1.5V; E_E 3V in H_2SO_4 0.05 M, while E_I 2V; E_E 3.5 V in H_2SO_4 0.5 M results in relatively transparent, ordered, large, and thin graphene flakes (Figure 2a and d). Well-ordered hexagonal graphite lattices of multi-layered EGO flakes are observed for EGO samples prepared at E_I 2V; E_E 3.5 V in H_2SO_4 0.05 M (Figure S2j), indicating an increase in the structural order of the EGO sheets with increasing E_E and E_I. Some regions exhibit buckling or wrinkling, as observed in Figures S2a-l. These effects can be explained by the thermodynamic stability of the 2-D structure of graphene.[46,48] High-resolution transmission electron microscopy (HR-TEM) investigations substantiated that the EGO sheets were found in a range from few layers to multilayers of GO (depicted in Figures S3 to S6). A representative HR-TEM image of a few layers of EGO, featuring an interlayer spacing of around 3.62 Å, is illustrated in Figure S6a. Furthermore, the EGO power spectra (Figure S3-6) display diffraction signals from various planes of graphene material distinctive to few layers and multilayers of GO materials.

The thickness of the graphene stacks prepared was further investigated using atomic force microscopy (AFM). An EGO suspension prepared by applying 2V intercalation potential (E_I) and 3.5V exfoliation potential (E_E) in 0.05 M, 0.1 M, and 0.5 M H_2SO_4 (Figure 3a, b and c respectively) solutions was drop-casted onto a silicon wafer surface for AFM analysis. The silicon surface was chosen as a reference surface for morphological investigations due to its flatness. Diverse sizes and thicknesses of EGO sheets were evident in treatments T4. The EGO sheet areas ranged from 0.1 to 10 µm², whereas their thicknesses were observed to span from 0.5 nm to 4 nm, as depicted in Figure S7. This electrochemical method has the capability to create EGO nanosheets with different shapes. The z-height profile of Figure 3 reveals that the height of the EGO flakes is between 0.5 and 4 nm, indicating the presence of few-layer and multilayer structures within the stacks. By using high E_I and E_E values and employing the centrifugation method few-layer thick EGO flakes can be produced and separated from larger flakes.

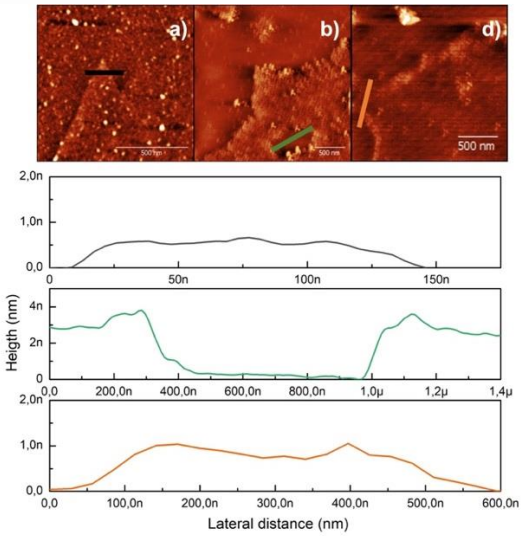

Figure 3. Tapping mode AFM images with their corresponding height profiles for EGO T4 (E_I 2V; E_E 3.5V) in H_2SO_4 **a)** 0.05 M **b)** 0.1M and **c)** 0.5M.

Raman and XPS measurements were conducted to assess the presence of defects and oxygen functional groups in the samples. XPS analysis was employed to characterize the EGO materials produced in this study and to obtain surface information following different treatments (T1 - T4, as outlined in Table 1). One of our specific goals is to evaluate the quantity of oxygen- and sulfur-containing functional groups, as these groups are known to

significantly influence the electrochemical properties of EGO flakes.

XPS survey spectra (Figure S8) exhibit the expected peaks corresponding to C 1s (285 eV) and O 1s (532 eV). Additionally, the S 2p peak (164 eV) indicates the incorporation of sulfur dopants in the samples. [36,49] The different treatments yielded EGO materials with oxygen content ranging from approximately 18% to 36% and sulfur content ranging from 3% to 12% (Table S1). Notably, the oxygen content in the EGO samples synthesized through successive intercalation-exfoliation steps in diluted H_2SO_4 solutions decreased as the treatment conditions became more severe, remaining relatively constant between 18% to 22%. Conversely, the sulfur content in the EGO samples did not exhibit a clear trend across the different treatments (Figure 4b). Compared to the Hummers' method, the proposed methodology yielded EGO materials that were slightly less oxidized, as evidenced by C/O ratios ranging from 1.5 to 4.3 (Figure 4a).[50] Treatment T3 (E_I = 2.0V, E_E= 3.0V) produced EGOs with a high C/O ratio (>4) and a low sulfur content (<4 at %). This electrochemical approach involving anodic potentials in dilute H_2SO_4 solutions (<0.5 M) favored the production of oxygenated groups and functionalization with sulfate ions during the intercalation-exfoliation process.[35,36]

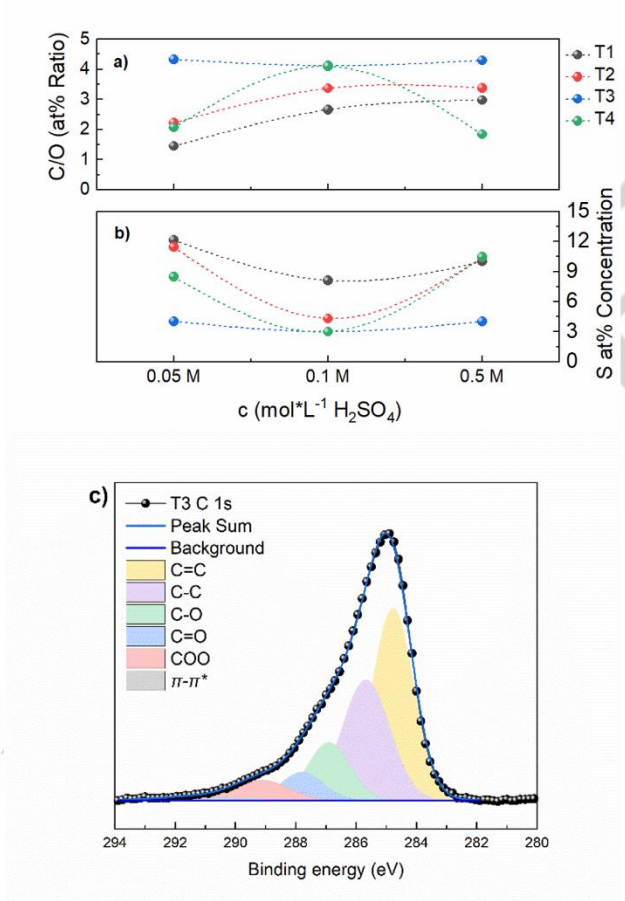

Figure 4. C/O at% ratio a) and Sulfur (S at%) percentage b) trends with varying H2SO4 concentration in XPS for EGO materials and c) High-resolution C1s XPS spectra of the EGO materials (T3 in H_2SO_4 0,5M). Peak-fitting results correspond to different functional groups.

Furthermore, the C 1s high-resolution spectrum was subjected to deconvolution analysis, identifying six distinct components (Figure 4c) corresponding to different carbon species. At 284.5 eV, a peak attributed to sp^2 hybridized carbon atoms in the graphene sheets was observed. Another peak, around 285.2 eV, was associated with sp^3 hybridized carbons, including C-C, C-H, and C vacancies. A peak at 286.3 eV indicated the presence of C-O groups, specifically hydroxyl and epoxide functional groups. A peak at 287.8 eV was assigned to carbonyl groups (C=O). And another two peaks at 289.1 eV and 290.8 eV corresponding to O-C=O and π- π* satellite bonds, respectively.[32,44,49] The relative percentages of these carbon species were quantitatively analyzed, and the results are depicted in Figure S9-S10. Notably, the sp^2 peak corresponding to intact graphene structures exhibited prominence across the different treatments, principally when higher intercalation-exfoliation potentials were applied with various acid concentrations.

The O 1s spectra (Figure S11) of samples obtained using treatments T1, T2, T3, and T4 with 0.05, 0.1, and 0.5 M concentrations, were deconvoluted up to five components: semiquinone (SQ), C=O, C–O, COO, and O_2/CO_2.[51,52] Semiquinones mostly prevail in samples treated in lower concentrations. This finding will come in handy when the S 2p spectra are also analyzed. The S 2p spectra (Figure S12) confirm the presence of covalent sulfates (SO_x) in all samples.[53] The binding energies for the components S=O and S–O in covalent sulfates overlap with those of C=O and C–O, which renders the analysis of O 1s XPS in terms of C vs. S bonding not so straightforward .[54] Each S 2p spectrum was plausibly fit to one component. However, scrutiny on shifts of the S 2p peak position and width informs about a relation between these groups' formation and acid concentration. Figure S13a demonstrates that for each treatment, as the concentration of H_2SO_4 increases, the S 2p binding energy increases, the S 2p width decreases, and SQ diminishes. This effect is ambiguous and requires thorough future investigation. However, there is another plausible explanation. The chemical environment surrounding covalent sulfates can influence S-O binding energy. As demonstrated in Figure S13b, neighboring electron-withdrawing groups such as the oxygen functionalities, introduced by the oxidation process, can interact with the electron density of the covalent sulfate group. The closer the covalent sulfate is to the oxygen functionalities, the lower is the electron density of the covalent sulfate, and the higher is the binding energy of the covalent sulfate group. The distribution of the oxygen functionalities and the homogeneity of their separation from covalent sulfate groups dictate how distributed the chemical states (FWHM)[55] of covalent sulfates are. Therefore, it is reasonable to assume that as the concentration increases, there is an increase in the homogeneity of oxygen functionality distribution, and more spatially compact covalent sulphates and oxygen functionalities state emerges. In this study, the electrochemical intercalation-exfoliation of graphite in H_2SO_4 showcased the capability to produce EGO materials with a controllable C/O ratio by modulating the I-E conditions. This approach offers notable advantages, including reduced processing times and elimination of hazardous chemicals. The presence of oxygen and sulfur groups in EGO holds great promise for a wide range of applications, encompassing composite material production and electroanalytical platforms.

Raman spectroscopy is a non-destructive technique that can be applied to study carbon materials as regards their structure, defects, and layer characteristics with sp^2 hybridization, including its allotropes. Raman spectra of carbon materials typically exhibit three prominent bands: the G band (1580 cm^{-1}), the D band (1350

cm^{-1}), and the 2D band (2700 cm^{-1}), as depicted in Figure 5. The D band arises from defects or disorders in the sp^2 structure, primarily attributed to the radial breathing modes of carbon atoms in aromatic rings. In addition, a minor band referred to as the D' band can be observed as a shoulder in the high-frequency region of the G band. The intense and narrow G band, which does not require aromatic rings, indicates graphitic order and results from the relative movement of carbon atom pairs bonded by sp^2 bonds. Positions of these bands, as well as peak width, and relative intensities provide valuable information about the characteristics of the material.[56]

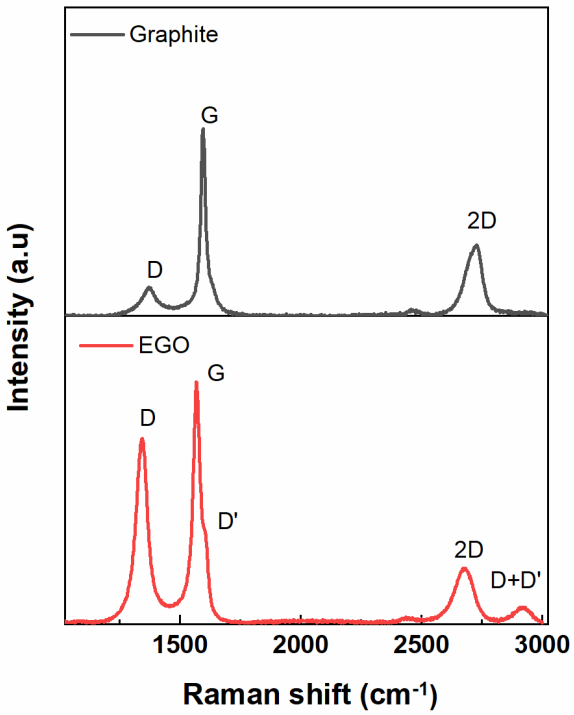

Figure 5. Raman spectra of graphite and EGO (T3 in H_2SO_4 0,5M)

The I_D/I_G ratio, representing the intensity ratio of the D and G bands, is commonly employed to assess the degree of structural disorder within the graphitic network. An increase in the I_D/I_G ratio indicates a higher disorder. The 2D band, an overtone of the D band, varies in shape depending on the number of graphene layers present. The I_{2D}/I_G ratio serves as an indicator of the layer count in graphene-like materials.[56–58] Figure 5 shows the Raman spectrum of graphite in black, exhibiting a narrow and intense G band at 1575 cm^{-1} and a weak D band at 1350 cm^{-1}. The I_D/I_G ratio is 0.11, indicating a low defect content. In contrast, the red trace corresponds to graphene-like material obtained through the electrochemical I-E (T3 in H_2SO_4 0,5M) process that displays an I_D/I_G ratio of 0.79. The appearance of a D' band at 1615 cm^{-1} confirms the defects resulting from the applied treatment for the synthesis of the material.

The influence of different treatments on the material quality was assessed by using the I_D/I_G (Figure 6a). Graphite exhibits an I_D/I_G value of 0.11 while chemically synthesized graphene oxide by using the Hummers' method typically displays I_D/I_G values ranging from 1.01 to 1.2.[15,23,25,50] In this study, the employed E_I and E_E method produced EGO flakes with a lower defect content (I_D/I_G ratio < 1.2), influenced by the concentration of the exfoliating electrolyte and the treatment applied. The increased I_D/I_G value suggests the introduction of SO_4^{2-} groups during exfoliation, leading to disorder in the carbon bonds. The I_D/I_G ratio values for the EGO materials obtained in this study range from 0.55 to 0.78 for high H_2SO_4 concentrations and from 0.7 to 1.1 for lower acid concentrations (Figure 6a). These values indicate an increase in defects as the treatment becomes less intense and a decrease in defects when the treatment is more aggressive.

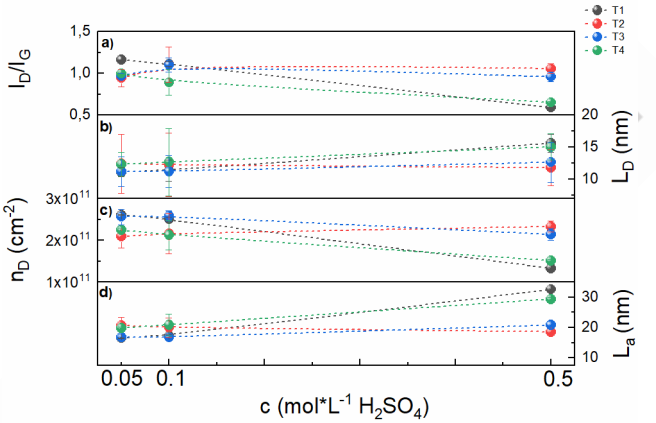

Figure 6. a) Variation of I_D/I_G ratio with the electrolyte solution concentration for different electrochemically assisted exfoliation and intercalation treatments, **b)** same as a) for the average defect distance (L_D), **c)** same as a) for the defect density (n_D) and **d)** same as a) for the size of nanocrystallites (L_a).

The enhanced intensity of the D band signal further supports the treatment-dependent presence of defects in the material. It is worth noting that the I_D/I_G ratio is commonly utilized to estimate the size of nanocrystallites (L_a) - see Figure 6d - and the presence of point defects in the sp^2 carbon lattices. The average defect distance (L_D) -see Figure 6b - and defect density (n_D, cm^{-2}) – see Figure 6c - can be determined by using the approach proposed by Tuinstra and Koenig and the modifications suggested by Cançado et al.[57,58] The following equations were employed to calculate these parameters:

$$L_a\,(nm) = 2.4x10^{-10}(\lambda_L)\left(\frac{I_D}{I_G}\right)^{-1} \quad (1)$$

$$L_D^2(nm^2) = 1.8x10^{-9}\lambda_L^4\left(\frac{I_D}{I_G}\right)^{-1} \quad (2)$$

$$n_D(nm^{-2}) = \frac{1.8x10^{22}}{\lambda_L^4}\left(\frac{I_D}{I_G}\right) \quad (3)$$

Where, λ_L is the wavelength of the Raman laser source. By applying these equations to the Raman spectroscopy data, we can gain valuable insights into the structural characteristics and quality of the carbon materials under investigation. The I_D/I_G ratio is a key parameter in determining nanocrystallite size and assessing the presence of defects, facilitating a comprehensive understanding of the properties and potential applications of the material. The empirical equations (1), (2), and (3) are applicable for point defects but not for edge defects, intercalants, and charged impurities, as these factors do not affect the intensity of the D-band. Figure 6 shows calculated values obtained from the empirical equations and Raman spectra of EGO samples. The trends observed in the I_D/I_G ratio and the calculated across-plane

and in-plane crystallite size (L_a) reveal that the size of the sp^2 crystallites or the number of sp^2 domains increase by approximately 25% with the increase in acid concentration for treatments T1 and T4, while for treatments T2 and T3, this increase is below 10%. Notably, for T1 and T4, a clear decrease in defect density (n_D), the quantity of defects ($I_D/I_G < 0.55$), and the distance between them (L_D) can be observed. Moreover, for acid concentrations ranging from low to moderate (< 0.1 M), it is evident that the defect density and the distance between defects are comparatively high compared to the previously mentioned conditions, and they remain relatively constant within the concentration range depicted in Figure 6.

Besides, the shape and intensity of the 2D band peak provides insight into the differences between graphitic and graphene-like materials. Figures S14a and b present Raman spectra in the 2D region for graphite and EGO, respectively. The presence of a single peak in the 2D band for the obtained material signifies the formation of GO, whereas, in graphite, the 2D band appears as the sum of two contributions, namely peaks at 2674 cm^{-1} and 2709 cm^{-1}. The appearance of a D+D' peak at approximately 2940 cm^{-1} corresponds to defects introduced by the intercalation of SO_4^{2-} ions, which are absent in non-intercalated graphite layers.[56]

As indicated, the shape of the peak around 2700 cm^{-1}, as shown in Figure S14b, exhibits a single contribution for the 2D band.[59] According to the literature, this result corresponds to few graphene layers, typically ranging from 5 to 15 (as shown in Figure 3). Increasing peak intensity with the treatment indicates decreased EGO layers in the exfoliated flakes. Therefore, as the treatment becomes more intense, thinner flakes with a higher defect content are obtained (also related with current-time transients oscillations discussed before), while decreasing the intensity of the treatment leads to thicker flakes with a lower defect content. In summary, the combined analysis of XPS, Raman spectroscopy, and AFM data reveals an interesting relationship between the C/O ratio, the presence of defects and the thickness of the EGO flakes. The treatments that exhibited higher C/O ratios also showed larger quantities of defects. Moreover, the analysis of the 2D band, HR-TEM and AFM data indicated the presence of a few layers of graphene. Thus, the presented study revealed useful information regarding the structural characteristics and quality of the EGO materials obtained under different treatment conditions.

Cyclic voltammetry (CV) and Electrochemical impedance spectroscopy (EIS) were employed to investigate the electrochemical behavior and charge transfer properties of the synthesized EGO materials. Figure 7a - d presents the CV curves obtained for EGO samples at scan rate of 50 mV/s in 1mM $[Fe(CN)_6]/K_4[Fe(CN)_6]$ + 0.1 M KCl solution. These results indicate the electrochemical process prevalent on the electrode for the different glassy carbon electrodes EGO (GCE-EGO) coated surfaces. As explained below, they provide important evidence that helps in ranking the comparative electrocatalytic performance of the modified electrodes towards the hexacyanoferrate (III)/(II) redox couple

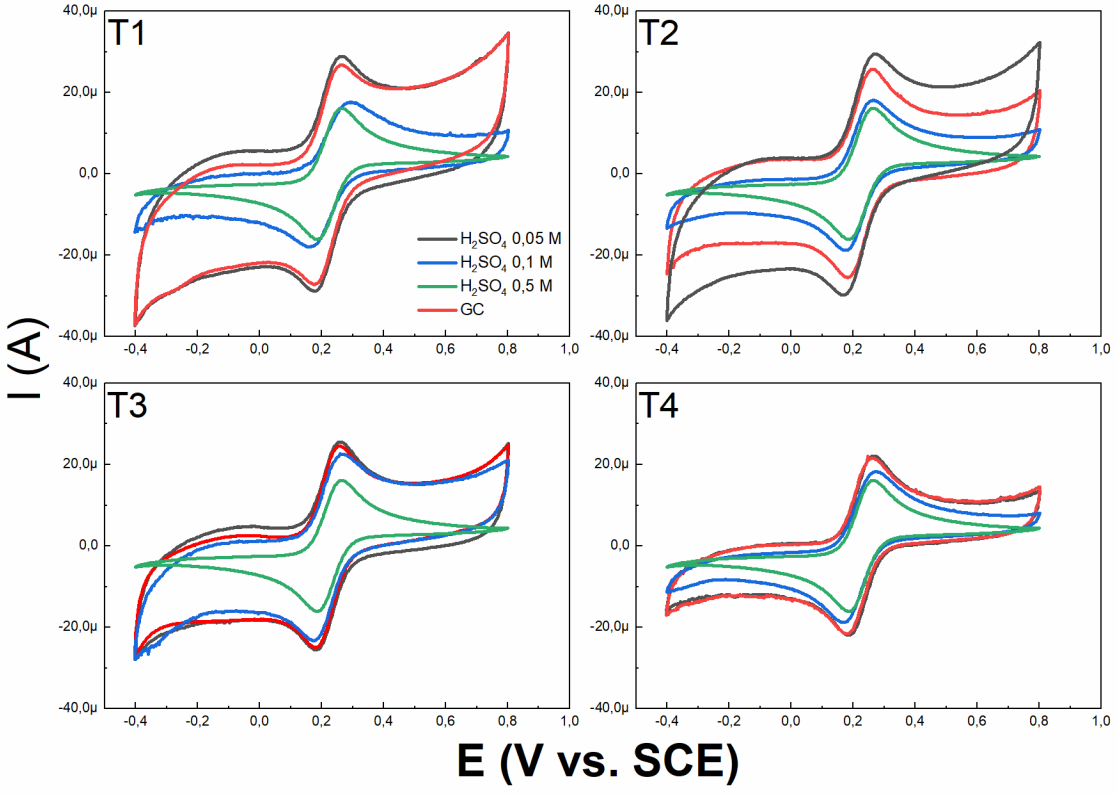

Figure 7. Representative cyclic voltammograms obtained with EGO- film-modified GCE in the presence of 1 mm ferro-/ferricyanide redox probe. Supporting electrolyte, 0.1m KCl; scan rate, 0.05 V s^{-1}; reference electrode, Ag/AgCl (3M KCl).

XPS and Raman analyses show that a rising amount of SO_4^{2-} ions into the electrolyte during I-E process, either by increasing anion concentration in the electrolyte (for a fixed E_I and E_E time) or by increasing E_I and E_E (at constant anion concentration in solution). Under such conditions, the change in the peak position (E_p), specifically the ΔE_p, can provide valuable information about the electrochemical behavior of EGO.[38,60,61]

The position of the ΔE_p, which represents the redox processes associated with the hexacyanoferrate (III)/(II) redox couple on GC-EGO covered electrodes, can be affected by various factors such as the oxidation state, surface functional groups, and structural characteristics of EGO. ΔE_p, in the CV curve of EGO (Figure 9b) corresponds to the reduction and oxidation of oxygen-containing functional groups, such as hydroxyl (-OH), epoxy (-O-), and carbonyl (C=O) groups, present on the surface of EGO as we discussed above in XPS results. The position of the ΔE_p, reflects the energy required for the electrochemical reactions associated with these functional groups. Changes in the oxidation state of EGO (oxidation or reduction), can lead to shifts in the delta ΔE_p. For example, an increase in the oxygen content (Figure 4a) or the presence of more oxidized functional groups can result in a shift towards higher potentials in the CV curve (Figure 9b) for EGO samples obtained here. Conversely, a reduction in the oxygen content or the presence of reduced functional groups can cause a shift towards lower potentials (Figure 9b). Differences in electrochemical performances of single- and few-layer graphene are marginal. The electrochemistry of EGO materials is strongly influenced by the amount of oxygen-containing groups on the EGO flakes.[61]

Electrochemical Impedance Spectroscopy (EIS) is a powerful technique used to investigate the interfacial properties of modified electrodes, specifically, in this case, GCE modified with various EGO materials. By measuring the impedance over a frequency range (0.01 Hz – 50 KHz), EIS provides insights into charge transfer processes and the conductivity of the EGO materials. The impedance data is typically represented by Nyquist plots, which exhibit a characteristic semicircular shape at high frequencies followed by a linear region at lower frequencies (Figure 8). The semicircular portion of the Nyquist plot represents the charge transfer resistance ($R_{c.t}$) associated with the electrode-electrolyte interface. A more negligible charge transfer resistance indicates more efficient electron transfer kinetics at the interface. The linear region of the plot corresponds to the Warburg diffusion impedance, which reflects the electroactive species diffusion processes occurring within the electrolyte. A linear region indicates semi-infinite linear diffusion ion transport through the EGO materials.[62–64]

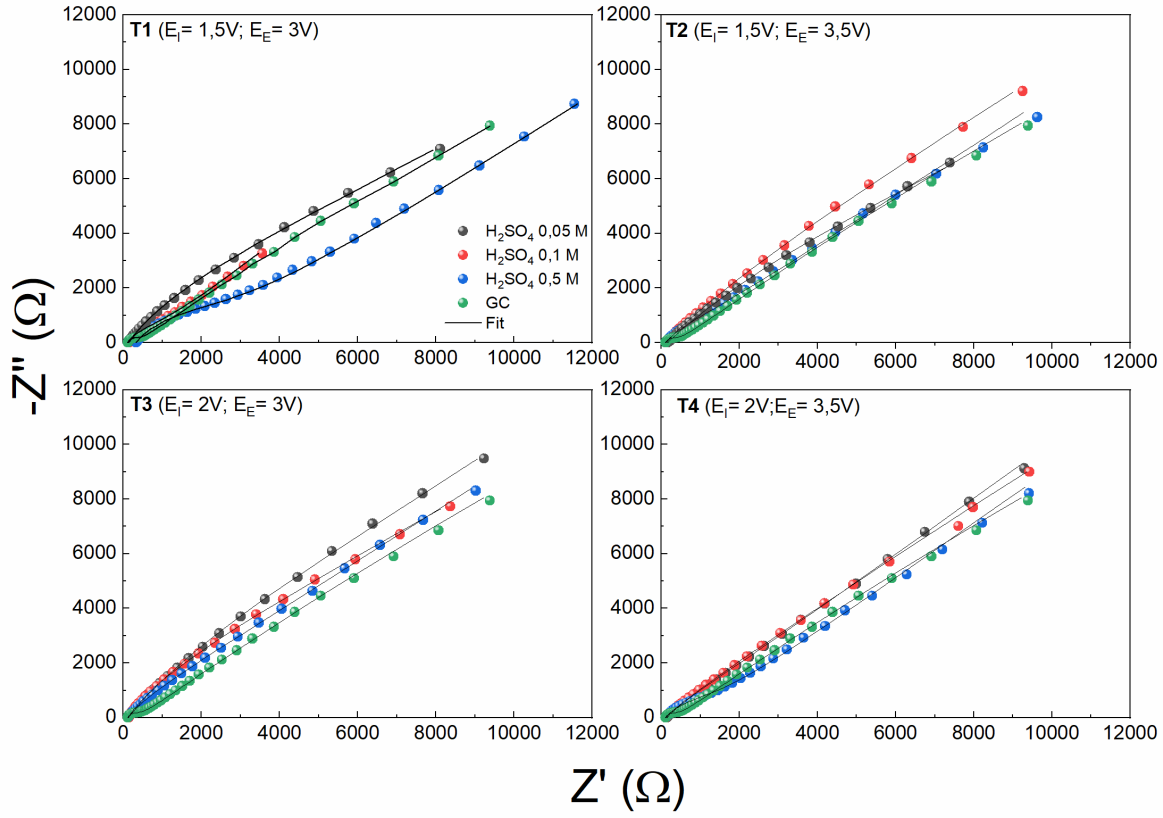

Figure 8. Nyquist diagrams for GCE/EGO in the presence of 1 mm ferro-/ferricyanide redox probe. Supporting electrolyte, 0.1M KCl. Solid line (—) correspond to the fitting of the experimental data.

To further analyze the EIS data, we employed an approach proposed by Casero et.al, by using complex non-linear least squares fitting of a theoretical impedance of an equivalent circuit to the experimental data.[63] The fitted circuit (Figure S15) includes various electronic elements representing different components. For example, R_e represents the electrolyte resistance, $R_{C.T}$ and CPE_1 correspond to the graphene surface without oxygen-containing functional groups, and CPE_2 and W_s represent the oxidized surface. The W_s element represents diffusion through an oxidized graphene structure, which includes different oxygen-containing groups such as C-OH, C-O, C=O, and O-C=O.

By fitting the equivalent circuit to the impedance diagrams, we obtained values for various parameters. The charge transfer resistance (R_{CT}) for the EGO-modified GCE increased compared to the unmodified GCE, indicating changes in the charge transfer kinetics. Conversely, the capacitance values showed the opposite trend.

Furthermore, we calculated the time constant ($\tau_{c.t}$) for the charge transfer process using the R_{CT} and $C_{d.l}$ (double layer capacity) values obtained from the fitting. The $\tau_{c.t}$ values, shown in Figure 9a, demonstrate a correlation with the defect density (n_D) and crystallite size (L_a). Samples with lower defect density and larger crystallite size exhibit shorter charge transfer times on the order of 10^{-4} s. In comparison, samples with higher defect density and smaller crystallite size show longer charge transfer times exceeding 1 s.

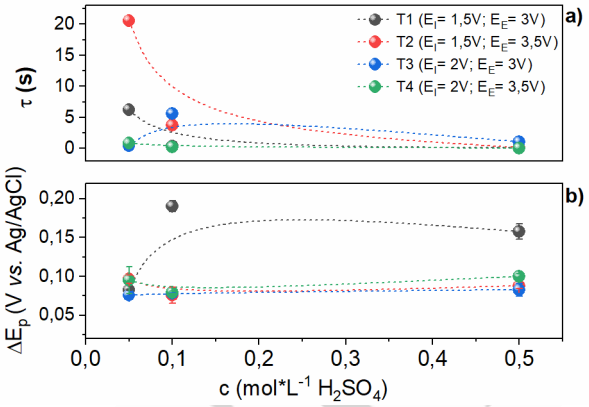

Figure 9. Parameters obtained from the electrochemical characterization a) The time constant of the charge transfer process from the EIS measurements and b) ΔE_p from the CV data.

Overall, the EIS analysis of the EGO materials reveals valuable information about their electrochemical performance, including charge transfer kinetics and ion diffusion processes. The observed trends in charge transfer resistance, capacitance, and charge transfer times highlight the influence of defect density and crystallite size on the electrical properties of the EGO-modified electrodes.

There are several works in literature dealing with the electrochemical exfoliation of graphene oxide (EGO), These studies have offered insights into various methodologies and techniques for achieving effective electrochemical exfoliation of GO.[65–71] However, the current article focusing on the Intercalation-Exfoliation process, differently from previous works, uniquely capitalizes on the combined I-E approach, harnessing its inherent benefits such as controlled layer separation, improved scalability, and enhanced exfoliation efficiency. By underscoring these differentiating factors, we highlight the potential of the approach for efficient GO exfoliation and subsequent applications. Table S2 shows a comparison of reaction parameters and properties of GO prepared by different methods.

Conclusion

In this study, we successfully synthesized graphene oxide (GO) using an electrochemical exfoliation method and comprehensively characterized its structural and electrochemical properties. The electrochemical exfoliation process involving intercalation and exfoliation potentials resulted in EGO materials with different degrees of oxidation, defect density, and crystallite size. XPS analysis revealed the presence of oxygen and sulfur functional groups in the EGO samples, with the oxygen content ranging from 18% to 36% and the sulfur content ranging from 3% to 12%. Raman spectroscopy provided insights into the defect density and layer characteristics of the EGO materials, with the I_D/I_G ratio indicating the presence of defects and the I_{2G}/I_D ratio indicating the layer count. TEM and AFM analysis confirmed the formation of EGO flakes with distinct layering, intercalation regions, and structural defects. Additionally, HR-TEM analysis demonstrated the preservation of multi to few layers of graphene oxide inferred from the interference and diffraction patterns. The electrochemical behavior of the synthesized EGO was investigated using CV and EIS measurements. The CV curves exhibited characteristic features associated with the oxidation and reduction of oxygen-containing functional groups on the EGO surface. The EIS results revealed low charge transfer resistances and high diffusion coefficients, indicating excellent electrochemical performance of the EGO materials. The correlations between the electrochemical properties and the structural characteristics of the EGO samples were established, highlighting the influence of oxidation degree, defect density, and crystallite size on the charge transfer kinetics and ion diffusion processes. Overall, the electrochemical exfoliation method presented in this study offers a promising approach for the production and characterization of EGO, providing insights into its potential applications in various fields.

Experimental Section

Materials

H_2SO_4 (95-97% P/P, δ=1.84gr/ml, MW=98.08) was obtained from Sigma-Aldrich and used without further treatment for the GO exfoliation. KCl, $K_3[Fe(CN)_6]$ and $K_4[Fe(CN)_6]$ were purchased from Sigma-Aldrich and used without further purification. All solutions were prepared with Milli-Q water. Graphite rods (99.999% purity) of 6 mm diameter were obtained from Sigma Aldrich.

Apparatus

All electrochemical procedures were recorded using an AUTOLAB PGSTAT204 (Metrohm Autolab B.V., The Netherlands) computer-controlled potentiostat, using a three-electrode system. A Pt plate and a saturated Ag/AgCl electrode were used as counter and reference electrodes respectively. Raman spectra were obtained using a Renishaw 2000 spectrometer equipped with three laser beams of 532, 633 and 785 nm, and a CCD camera detector, an inner calibration source and a digital sample holder controlled by Wire 2.0 software. XPS spectra were acquired in a SPECS Sage HR 100 spectrometer with a non-monochromatic source (Mg line Kα 1253.6 KeV, 250W of applied power and using the full width at half height maximum method of 1.1 eV for calibrating - with the 3d 5/2 silver line). All measurements were taken in a Ultra High Vacuum chamber (UHV) with a pressure below $5x10^{-8}$ mbar. Gaussian-Lorentzian functions were used to adjust data, after baseline correction. For microscopy images a Transmission Electron Microscopy JEOL JEM-1400PLUS (40 kV – 120 kV) was used with a GATAN US1000 CCD (2k x 2k) chamber, and an Image Plate System DITABIS (6k x 5k).

Procedures

The electrochemical exfoliation of graphite: The graphite rod was cut into pieces of about 1 cm in length and used as a working electrode connected to the anode employing a Cu alligator clip. A surface of about 0.5 cm was immersed in the electrolyte solution. Exfoliation was carried out using a two-step electrosynthesis technique, applying a lower potential first (intercalation process) followed by applying a higher potential (exfoliation step) in the presence of the H_2SO_4 electrolyte at different concentrations (0.05, 0.1 and 0.5 M). The intercalation values were 1.5V and 2.0V, while the exfoliation consisted of 3.0V and 3.5V. An experimental design of three factors randomly ordered was used to carry out the experiments (Table 1). The electro exfoliated GO (EGO) powder produced was collected by centrifugation, rinsed with bidistilled water until neutral pH and dried at 60ºC. The material was characterized by TEM, Raman and XPS.

Electrochemical characterization of GO: Solutions of 1mg of EGO in 1 mL of bidistilled water were prepared through sonication for 15 minutes. 3 mm glassy carbon discs (0.071 cm^2 geometric area) embedded in Teflon were mechanically polished by using a 0.3 mm alumina suspension and kept in water until the modification. Modified electrodes were prepared by dropping 5.0 µL of GO aqueous solution onto the surface of clean glassy carbon electrode (GCE), dried in an oven at 60°C, and rinsed with water thoroughly (denoted as EGO/GCE, hereafter). The electrochemical studies on the modified electrode were carried out in 0.1 M KCl solution containing 1 mM $K_3[Fe(CN)_6]/K_4[Fe(CN)_6]$ (1:1 molar ratio) also in a three-electrode system under nitrogen atmosphere, employing an Autolab PGSTAT 204 (Metrohm Autolab B.V., The Netherlands) potentiostat controlled by Nova 2.1 software. The CV responses were measured in a potential range from −0.4 V to 0.8 V (*vs*. Ag/AgCl) at a scan rate of 50 mV/s with consecutive three cyclic scans. Electrochemical impedance spectroscopy (EIS) was performed with the frequency range of 0.01 Hz – 50 kHz, operating potential of 0.20 V, and perturbation amplitude of 5 mV. Analysis of the data obtained during the electrochemical impedance measurements was performed by fitting the impedance of an equivalent circuit to the experimental spectra in the frame of the Nova facilities.

Acknowledgements

S.E.M. thanks the PID2020-114356RB-I00 project from the Ministry of Science and Innovation of the Government of Spain. This work was performed under the Maria de Maeztu Units of Excellence Program from the Spanish State Research Agency - Grant no. MDM-2017-0720. C.A. Gervasi duly acknowledges the Buenos Aires Commission for Scientific and Technological Research (CICPBA) as Senior Research Scientists in this Institution. Support of this work by the agency ANPCYT [grant number PICT2019- 2019- 00116] is explicitly acknowledged.

Keywords: Graphene Oxide • Intercalation • Exfoliation •

[1] M. Nehra, N. Dilbaghi, A. A. Hassan, S. Kumar, *Carbon-Based Nanomaterials for the Development of Sensitive Nanosensor Platforms*, Elsevier Inc., **2019**.
[2] F. D'Souza, K. M. Kadish, *Handbook of Carbon Nano Materials*, **2015**.
[3] M. Inagaki, F. Kang, in *Carbon Materials Science and Engineering: From Fundamentals to Applications*, Elsevier, **2014**.
[4] M. Thangamuthu, K. Y. Hsieh, P. V. Kumar, G. Y. Chen, *Int J Mol Sci* **2019**, *20*.
[5] J. Sturala, J. Luxa, M. Pumera, Z. Sofer, *Chemistry - A European Journal* **2018**, *24*, 5992–6006.
[6] A. K. Geim, K. S. Novoselov, *Nat Mater* **2007**, *6*, 183–191.
[7] B. L. Dasari, J. M. Nouri, D. Brabazon, S. Naher, *Energy* **2017**, *140*, 766–778.
[8] D. G. Papageorgiou, I. A. Kinloch, R. J. Young, *Prog Mater Sci* **2017**, *90*, 75–127.
[9] S. Zhang, H. Wang, J. Liu, C. Bao, *Mater Lett* **2020**, *261*.
[10] X. Zhou, F. Liang, *Curr Med Chem* **2014**, *21*, 855–869.
[11] M. H. Chakrabarti, C. T. J. Low, N. P. Brandon, V. Yufit, M. a. Hashim, M. F. Irfan, J. Akhtar, E. Ruiz-Trejo, M. a. Hussain, *Electrochim Acta* **2013**, *107*, 425–440.
[12] H. Beitollai, M. Safaei, S. Tajik, *International Journal of Nano Dimension* **2018**, *0*, 125–140.
[13] C. T. J. Low, F. C. Walsh, M. H. Chakrabarti, M. a. Hashim, M. a. Hussain, *Carbon N Y* **2013**, *54*, 1–11.
[14] S. K. Tiwari, S. Sahoo, N. Wang, A. Huczko, *Journal of Science: Advanced Materials and Devices* **2020**, *5*, 10–29.
[15] L. Shahriary, A. a. Athawale, *International Journal of Renewable Energy and Environmental Engineering* **2014**, *02*, 58–63.
[16] K. Raidongia, A. T. L. Tan, J. Huang, in *Carbon Nanotubes and Graphene: Edition 2*, Elsevier Inc., **2014**, pp. 341–374.
[17] B. Konkena, S. Vasudevan, *Journal of Physical Chemistry Letters* **2012**, *3*, 867–872.
[18] W. Liu, G. Speranza, *ACS Omega* **2021**, *6*, 6195–6205.
[19] Y. Lin, Z. Feng, L. Yu, Q. Gu, S. Wu, D. S. Su, *Chemical Communications* **2017**, *53*, 4834–4837.
[20] I. M. De la Fuente Salas, Y. N. Sudhakar, M. Selvakumar, *Appl Surf Sci* **2014**, *296*, 195–203.
[21] Z. Wang, P. Tammela, M. Strømme, L. Nyholm, **2015**, 3418–3423.
[22] L. Wu, W. Li, P. Li, S. Liao, S. Qiu, M. Chen, Y. Guo, Q. Li, C. Zhu, L. Liu, *Small* **2014**, *10*, 1421–1429.
[23] H. L. Poh, F. Šaněk, A. Ambrosi, G. Zhao, Z. Sofer, M. Pumera, *Nanoscale* **2012**, *4*, 3515–3522.
[24] F. Pendolino, N. Armata, in *SpringerBriefs in Applied Sciences and Technology*, Springer Verlag, **2017**, pp. 5–21.
[25] P. Feicht, J. Biskupek, T. E. Gorelik, J. Renner, C. E. Halbig, M. Maranska, F. Puchtler, U. Kaiser, S. Eigler, *Chemistry – A European Journal* **2019**, *25*.
[26] A. Ambrosi, M. Pumera, *Chemistry - A European Journal* **2016**, *22*, 153–159.
[27] X. You, J.-H. Chang, B. K. Ju, J. J. Pak, *J Nanosci Nanotechnol* **2011**, *11*, 5965–5968.

[28] L. Li, D. Zhang, J. Deng, Q. Kang, Z. Liu, J. Fang, Y. Gou, *J Electrochem Soc* **2020**, *167*, 155519.
[29] J. Cao, P. He, M. A. Mohammed, X. Zhao, R. J. Young, B. Derby, I. A. Kinloch, R. A. W. Dryfe, *J Am Chem Soc* **2017**, *139*, 17446–17456.
[30] G. M. Morales, P. Schifani, G. Ellis, C. Ballesteros, G. Martínez, C. Barbero, H. J. Salavagione, *Carbon N Y* **2011**, *49*, 2809–2816.
[31] A. J. Cooper, N. R. Wilson, I. a. Kinloch, R. a W. Dryfe, *Carbon N Y* **2014**, *66*, 340–350.
[32] C.-Y. Su, A.-Y. Lu, Y. Xu, F.-R. Chen, A. N. Khlobystov, L.-J. Li, *ACS Nano* **2011**, *5*, 2332–9.
[33] F. Liu, C. Wang, X. Sui, M. A. Riaz, M. Xu, L. Wei, Y. Chen, *Carbon Energy* **2019**, *1*, 173–199.
[34] M. Alanyalioğlu, J. J. Segura, J. Oró-Sol, N. Casañ-Pastor, in *Carbon N Y*, Elsevier Ltd, **2012**, pp. 142–152.
[35] S. E. Lowe, G. Shi, Y. Zhang, J. Qin, L. Jiang, S. Jiang, M. Al-Mamun, P. Liu, Y. L. Zhong, H. Zhao, *Nano Materials Science* **2019**, *1*, 215–223.
[36] H. Lee, J. Il Choi, J. Park, S. S. Jang, S. W. Lee, *Role of Anions on Electrochemical Exfoliation of Graphite into Graphene in Aqueous Acids*, **2020**.
[37] P. M. Biranje, J. Prakash, A. P. Srivastava, S. Biswas, A. W. Patwardhan, J. B. Joshi, K. Dasgupta, *J Mater Sci* **2021**, *56*, 19383–19402.
[38] A. Ambrosi, C. K. Chua, A. Bonanni, M. Pumera, *Chem Rev* **2014**, *114*, 7150–7188.
[39] W. W. Liu, A. Aziz, *ACS Omega* **2022**, *7*, 33719–33731.
[40] Z. Shi, P. He, N. Wang, Y. Liu, X. Chen, Y. Li, G. Ding, Q. Yu, X. Xie, *Adv Funct Mater* **2022**, *32*.
[41] F. Beck, J. Jiang, H. Krohn, *Journal of Electroanalytical Chemistry* **1995**, *389*, 161–165.
[42] B. Gurzęda, T. Buchwald, M. Nocuń, A. Bąkowicz, P. Krawczyk, *RSC Adv* **2017**, *7*, 19904–19911.
[43] A. A. Papaderakis, A. Ejigu, J. Yang, A. Elgendy, B. Radha, A. Keerthi, A. Juel, R. A. W. Dryfe, *J Am Chem Soc* **2023**, *145*, 8007–8020.
[44] G. Ljubek, D. Čapeta, I. Šrut Rakić, M. Kraljić Roković, *J Mater Sci* **2021**, *56*, 10859–10875.
[45] Y. Nishina, S. Eigler, *Nanoscale* **2020**, *12*, 12731–12740.
[46] S. Rubino, S. Akhtar, K. Leifer, *Microscopy and Microanalysis* **2016**, *22*, 250–256.
[47] Y. C. Shin, M. S. Dresselhaus, J. Kong, *Preparation of Graphene with Large Area*, Elsevier Ltd, **2014**.
[48] G. Yang, L. Li, W. B. Lee, M. C. Ng, *Sci Technol Adv Mater* **2018**, *19*, 613–648.
[49] R. Al-Gaashani, A. Najjar, Y. Zakaria, S. Mansour, M. A. Atieh, *Ceram Int* **2019**, *45*, 14439–14448.
[50] H. Yu, B. Zhang, C. Bulin, R. Li, R. Xing, *Sci Rep* **2016**, *6*, 1–7.
[51] A. Subrati, P. Florczak, B. Gurzęda, E. Coy, J. Jenczyk, M. Kościński, B. Peplińska, S. Jurga, P. Krawczyk, *Carbon N Y* **2021**, *176*, 327–338.
[52] R. Larciprete, S. Fabris, T. Sun, P. Lacovig, A. Baraldi, S. Lizzit, *J Am Chem Soc* **2011**, *133*, 17315–17321.
[53] J. Hwang, S. J. Ha, A. Ramadoss, K. Y. Yoon, J. H. Jang, *ACS Appl Energy Mater* **2020**, *3*, 4348–4355.
[54] C. Petit, M. Seredych, T. J. Bandosz, *J Mater Chem* **2009**, *19*, 9176–9185.
[55] M. Smith, L. Scudiero, J. Espinal, J. S. McEwen, M. Garcia-Perez, *Carbon N Y* **2016**, *110*, 155–171.
[56] V. Nagyte, D. J. Kelly, A. Felten, G. Picardi, Y. Y. Shin, A. Alieva, R. E. Worsley, K. Parvez, S. Dehm, R. Krupke, S. J. Haigh, A. Oikonomou, A. J. Pollard, C. Casiraghi, *Nano Lett* **2020**, *20*, 3411–3419.
[57] L. G. Cançado, A. Jorio, E. H. M. Ferreira, F. Stavale, C. A. Achete, R. B. Capaz, M. V. O. Moutinho, A. Lombardo, T. S. Kulmala, A. C. Ferrari, *Nano Lett* **2011**, *11*, 3190–3196.
[58] L. G. Cançado, M. G. Da Silva, E. H. Martins Ferreira, F. Hof, K. Kampioti, K. Huang, A. Pénicaud, C. A. Achete, R. B. Capaz, A. Jorio, *2d Mater* **2017**, *4*.
[59] A. Kaniyoor, S. Ramaprabhu, *AIP Adv* **2012**, *2*.
[60] D. a. C. Brownson, J. P. Metters, D. K. Kampouris, C. E. Banks, *Electroanalysis* **2011**, *23*, 894–899.
[61] M. Pumera, *Electrochem commun* **2013**, *36*, 14–18.
[62] Y. Yoon, J. Jo, S. Kim, I. G. Lee, B. J. Cho, M. Shin, W. S. Hwang, *Nanomaterials* **2017**, *7*.
[63] E. Casero, A. M. Parra-Alfambra, M. D. Petit-Domínguez, F. Pariente, E. Lorenzo, C. Alonso, *Electrochem commun* **2012**, *20*, 63–66.
[64] A. F. Sardinha, D. A. L. Almeida, N. G. Ferreira, *Journal of Materials Research and Technology* **2020**, *9*, 10841–10853.
[65] J. Liu, H. Yang, S. G. Zhen, C. K. Poh, A. Chaurasia, J. Luo, X. Wu, E. K. L. Yeow, N. G. Sahoo, J. Lin, Z. Shen, *RSC Adv* **2013**, *3(29)*, 11745–11750.
[66] M. Hofmann, W. Y. Chiang, T. D Nguyn, Y. P. Hsieh, *Nanotechnology* **2015**, *26*.
[67] K. Parvez, R. Li, S. R. Puniredd, Y. Hernandez, F. Hinkel, S. Wang, X. Feng, K. Müllen, *ACS Nano* **2013**, *7*, 3598–3606.
[68] K. Parvez, Z. S. Wu, R. Li, X. Liu, R. Graf, X. Feng, K. Müllen, *J Am Chem Soc* **2014**, *136*, 6083–6091.
[69] K. Parvez, R. A. Rincón, N. E. Weber, K. C. Cha, S. S. Venkataraman, *Chemical Communications* **2016**, *52*, 5714–5717.
[70] J. Zhong, W. Sun, Q. Wei, X. Qian, H. M. Cheng, W. Ren, *Nat Commun* **2018**, *9*.
[71] W. Xu, W. Zhu, J. Shen, M. Kuai, Y. Zhang, W. Huang, W. Yang, M. Li, S. Yang, *Nanoscale* **2023**, *15*, 5919–5926.

Table of Contents

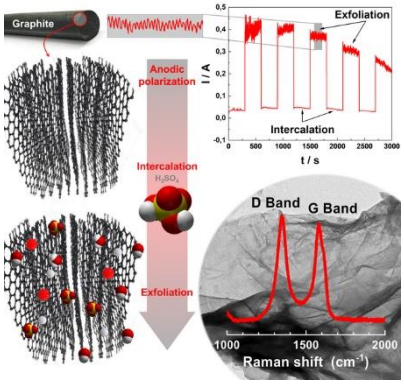

Between the sheets: The Intercalation-Exfoliation (I-E) method was successfully applied to produce graphene oxide (GO) materials with adjustable oxidation levels, defect density, and crystallite size by tuning applied potential and electrolyte concentration. Investigating the electrochemical properties of these GO samples via CV and EIS measurements with a selected redox probe establishes meaningful correlations between their structural features and performance, advancing our comprehension of their behavior.